Molecular Photobleaching Kinetics of Rhodamine 6G by One- and Two-Photon Induced Confocal Fluorescence Microscopy

Christian Eggeling,*[a] Andreas Volkmer,*[b] and Claus A. M. Seidel*[c]

Under high-excitation irradiance conditions in one- and two-photon induced fluorescence microscopy, the photostability of fluorescent dyes is of crucial importance for the detection sensitivity of single molecules and for the contrast in fluorescence imaging. Herein, we report on the dependence of photobleaching on the excitation conditions, using the dye Rhodamine 6G as a typical example. The different excitation modes investigated include 1) one-photon excitation into the first-excited singlet state in the range of 500 to 528 nm by continuous wave and picosecond-pulsed lasers and 2) two- and one-photon excitation to higher-excited singlet states at 800 and 350 nm, respectively, by femtosecond pulses. Experimental strategies are presented, which allow resolving the photophysics. From single-molecule trajectories and fluorescence correlation spectroscopy, as well as with a simple theoretical model based on steady-state solutions of molecular rate equation analysis, we determined the underlying photobleaching mechanisms and quantified the photokinetic parameters describing the dependence of the fluorescence signal on the excitation irradiance. The comparison with experimental data and an exact theoretical model show that only minor deviations between the different theoretical approaches can be observed for high-pulsed excitation irradiances. It is shown that fluorescence excitation is in all cases limited by photolysis from higher-excited electronic states. In contrast to picosecond-pulsed excitation, this is extremely severe for both one- and two-photon excitation with femtosecond pulses. Furthermore, the photostability of the higher-excited electronic states is strongly influenced by environmental conditions, such as polarity and temperature.

1. Introduction

Light microscopy with fluorescence detection has received a prominent place in life sciences because of its ability for quantitative functional imaging of biological processes with high three-dimensional spatial resolution, high sensitivity and specificity. This success is based on the recent interrelated advancements in molecular biology, chemistry, photophysics, spectroscopy and microscope technology.[1–5] Recent years have witnessed a renaissance of fluorescence microscopy techniques and applications, from live-animal multiphoton confocal microscopy to single-molecule fluorescence spectroscopy and imaging in living cells.[6–9] In particular, the use of confocal microscopes with laser excitation has provided the main prerequisite for single-molecule fluorescence spectroscopy in solution, that is, the limitation of the excitation and observation volume combined with efficient excitation and detection of the sample.[10–16] These features have offered the direct observation of fluorescence bursts and fluorescence fluctuations from single dye molecules diffusing through the focal femtolitre-sized detection volume.

In order to go beyond the mere localization of a molecule in three-dimensional space, various fluorescence spectroscopic methods such as fluorescence correlation spectroscopy (FCS),[17,18] fluorescence intensity distribution analysis (FIDA),[19–21] fluorescence lifetime imaging (FLIM)[22–26] and fluorescence recovery after photobleaching (FRAP)[27,28] have been applied, providing additional information about, for example, the molecule number, the mobility and molecular interactions and dynamics.[29] Recently multi-parameter fluorescence detection (MFD) has been introduced, which allows the simultaneous collection of all fluorescence parameters (i.e., intensity, lifetime, anisotropy in two spectral ranges) with sub-nanosecond time resolution.[2,30] Confocal fluorescence microscopy with multi-parameter fluorescence detection (MFD) harbors the potential of functional imaging by the complete use of fluorescence information in an at least eight-dimensional parameter space.[2,31] MFD has also been successfully applied to study the structure and function of biomolecules by measuring the fluorescence energy transfer in real time with sub-nanometer spatial and sub-millisecond temporal resolution.[32–34]

In a laser-induced fluorescence microscope, the laser light is usually focused to a spot with a diameter of less than 1 μm producing high irradiances in the range of $kW\,cm^{-2}$ to $GW\,cm^{-2}$. This feature not only enables efficient one-photon

[a] *Dr. C. Eggeling*
Max-Planck-Institute for Biophysical Chemistry
Department of Nanobiophotonics, Am Fassberg 11
37077 Göttingen (Germany)
Fax: (+49) 551-201-1085
E-mail: ceggeli@gwdg.de

[b] *Dr. A. Volkmer*
University of Stuttgart, 3rd Institute of Physics
Pfaffenwaldring 57, 70550 Stuttgart (Germany)
Fax: (+49) 711-685-5281
E-mail: a.volkmer@physik.uni-stuttgart.de

[c] *Prof. Dr. C. A. M. Seidel*
Heinrich-Heine-University Düsseldorf
Lehrstuhl für molekulare physikalische Chemie, Universitätsstr.1
40225 Düsseldorf (Germany)
Fax: (+49) 211-81-12803
E-mail: cseidel@gwdg.de

 DOI: 10.1002/cphc.200400509

excitation, but is also utilized for nonlinear optical microscopy techniques. These techniques rely on nonlinear interactions of preferably pulsed laser light with particular molecules in the biological sample. Such fluorescent molecules are either naturally present or have been introduced by genetic or other means. The most commonly used nonlinear process is two-photon excitation of fluorescence, which involves the nearly simultaneous absorption of two near-infrared photons.[1,35] Recently, even three-photon excitation has gained interest.[36–38] A near-infrared laser can be employed as the excitation source for multi-fluorophore multi-photon excitation and hence multi-color imaging. The introduction of dual-color cross-correlation and coincidence analysis coupled with fluorescence correlation spectroscopy has further expanded the utility of these techniques to encompass a wide range of promising applications in living cells.[39,40]

In order to achieve a high-fluorescence photon flux allowing for high scanning rates and high time resolution in spectroscopy, high irradiances for one and multiphoton excitations are typically applied in both scanning microscopy and confocal single-molecule spectroscopy. However, the photophysics of the dye labels bear limitations due to the high irradiances applied, namely a limitation in the fluorescence signal due to singlet and triplet saturation as well as photobleaching.[41,42] Recent work on the laser dye Rhodamine 6G (Rh6G) has shown that even for continuous wave (cw) one-photon excitation at 515 nm only a five-level molecular electronic state model, which takes photobleaching from higher-excited electronic states into account, is able to describe the dependence of photobleaching on the irradiance.[43] The photophysical and photochemical properties of Rh6G have been extensively studied by ensemble and single-molecule spectroscopies applying one- as well as two-photon excitation.[43–57] Two dark states were identified as important intermediates in the complex nonexponential photobleaching kinetics, that is, the triplet state and a radical anion. In addition, secondary photobleaching after optical excitation of those dark states was observed. Because higher electronic-excited states couple quite efficiently with ionic states in polar solvents such as water, two- and multistep absorption processes open additional channels for photobleaching.[58–62] This two-step photolysis is readily obtained with cw or pulsed lasers, as shown previously in the case of coumarins,[63–65] rhodamines,[43,51,54,66,67] fluorescein,[51] fluorescent proteins,[67,68] and other fluorophores.[64] The photobleaching following pulsed excitation depends on the peak irradiance as well as on the repetition rate.[54,63,65] Reactions of the metastable states with oxygen can lead either to photoproducts or to a recovery of the ground state. Oxygen can therefore enhance or reduce photobleaching, depending on the experimental conditions.[42,48,57,67] In this context, the complex effects of several chemical stabilizers such as L(+)-ascorbic acid (vitamine C), γ-L-glutamyl-L-cysteinyl-glycine (glutathione), 1,4-diazabicyclo[2,2,2]octane (DABCO), and 2-mercaptoethylamine (MEA, cysteamine) can be understood.[42,67]

Taking the dye Rh6G as a typical example for a label frequently used in fluorescence microscopy, this work presents several techniques, which provide new detailed insights into the influence of laser excitation conditions and the molecular environment of the label on the photobleaching processes. We report on photobleaching measurements of Rh6G in water under the conditions of one- and two-photon fluorescence microscopy. The different excitation modes investigated include 1) one-photon excitation into the S_1 state at 500 to 528 nm by continuous wave and picosecond-pulsed lasers; and 2) two- and one-photon excitation into higher-excited singlet states at 800 and 350 nm, respectively, by femtosecond-pulsed lasers. From single-molecule trajectories and FCS curves we determine the underlying photobleaching mechanisms and quantify the photokinetic parameters describing the fluorescence signal dependence on the excitation irradiance. Bleaching studies at low irradiances performed in a cell are complementing the experiments. In contrast to previous reports,[54,65] we employ a theory that is based on simple assumptions of steady-state populations and quasi-continuous irradiances in the case of pulsed excitation. Comparison to exact calculations show that the simplified model, nevertheless, describes all data remarkably well. From this model, optimal excitation conditions for single-molecule detection and fluorescence microscopy with respect to the number of emitted fluorescence photons and to the signal-to-background ratio can be deduced. It is important to note that the additional photobleaching due to two-step photolysis limiting the applicable irradiance greatly depends on the molecular environment such as the exposure of the fluorophore to water and the solvent polarity.[42,55,57,69–73]

2. Molecular Photokinetic Model of Photobleaching

Our photophysical model of photobleaching of Rh6G is based on an energy diagram consisting of five electronic levels.[42,43] Figure 1a depicts the ground singlet state, S_0, the first-excited singlet state, S_1, the lowest-excited triplet state, T_1, and higher-excited singlet and triplet states, S_n and T_n ($n>1$), respectively. The analysis of the one- and two-photon absorption spectra of Rh6G in water[36] and of the anisotropy spectrum in glycerol reveals three distinct electronic transitions in the spectral range between 320 and 600 nm (Figure 1b). The higher-excited singlet states, $S_{>1}(400)$ and $S_{>1}(350)$, which are populated by two- and one-photon excitation at 800 and 350 nm, respectively, are kinetically coupled to S_1 due to fast internal conversion (dotted lines). The $S_{>1}(400)$ state has a weak one-photon but strong two-photon cross-section.[36]

Excitation processes from states *i* to *f* are quantified by the rate constants $k_{(T)if}$; that is, k_{01} (S_0 to S_1), k_{1n} (S_1 to S_n), and k_{T1n} (T_1 to T_n). For one-photon excitation, $k_{(T)if}$ is proportional to the applied excitation irradiance, I (W cm^{-2}), and the corresponding absorption cross-section, $\sigma_{(T)if}(\lambda)$ (in cm^2), at the excitation wavelength, λ, as shown in Equation (1):

$$k_{(T)if}(\lambda) = \sigma_{(T)if}(\lambda)\, I\, \gamma \qquad (1)$$

$\gamma = \lambda/(hc_l)$ depicts the reciprocal photon energy, where h is Planck's constant, and c_l is the velocity of light.

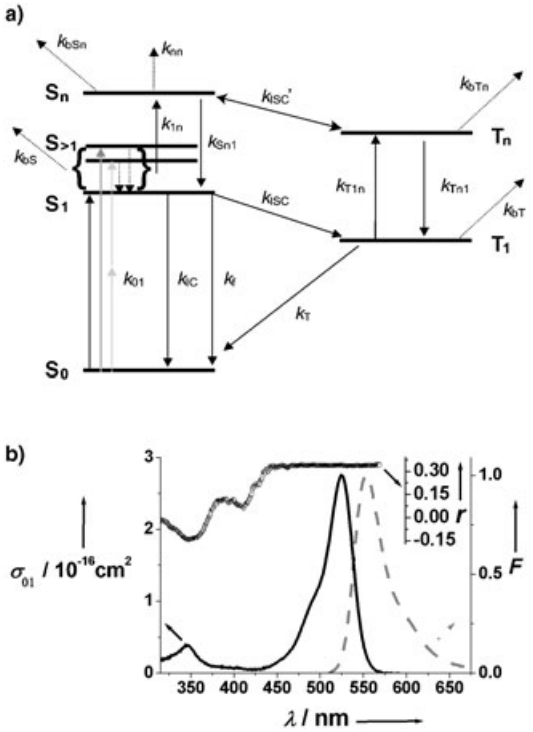

Figure 1. *a) Energy diagram of a dye molecule with five electronic levels including photobleaching reactions from each electronic excited state and different excitation modes with excitation rate, k_{01}; that is, excitation into S_1 at 502, 515 and 528 nm (black), one-photon excitation at 350 nm (grey) into the electronic singlet state, $S_{>1}(350)$, and two-photon excitation at 800 nm (light grey) into $S_{>1}(400)$, higher in energy than S_1, followed by fast (<ps) relaxation into S_1 (dotted). b) Absorption, σ_{01} (solid), and emission spectrum, F (dashed grey), of Rhodamine 6G in water with an absorption maximum at 524 nm and a fluorescence maximum at 552 nm. Furthermore, the fluorescence anisotropy spectrum, r (open dots), of Rhodamine 6G in glycerol is shown.*

For two-photon excitation, the two-photon absorption cross-section, $\delta_{(T)if}(\lambda)$ (in cm^{4}s), specifies the excitation rate, which exhibits a square dependence on the irradiance, [Eq. (2)]

$$k_{(T)if}(\lambda) = (\delta_{(T)if}(\lambda)/2)\, I^2\, \gamma^2 \qquad (2)$$

The factor 1/2 reflects the fact that two photons must be absorbed for each excitation event.[35,36,74,75]

Depopulation processes of each electronic excited state are characterized by the rate constants k_f, k_{IC}, and k_{ISC} for de-excitation of S_1 by fluorescence, internal conversion, and intersystem crossing to T_1, respectively, leading to an overall fluorescence lifetime of $\tau_0 = 1/k_0 = 1/(k_f + k_{IC} + k_{ISC})$. k_T, k_{Sn1}, and k_{Tn1} denote the de-excitation rate constants of T_1, S_n, and T_n, respectively. Rate constants for stimulated de-excitation and intersystem crossing between T_n and S_n states, k_{ISC}',[76] are assumed to be negligible for the dye Rh6G under the present experimental conditions. Furthermore, only the lowest vibronic level of each electronic state is considered, that is, fast relaxation from higher vibronic states is assumed.

Any photochemical reaction from excited electronic states where the dye irreversibly looses its fluorescence characteristic is denoted as photobleaching with the microscopic rate constants, k_{bS}, k_{bT}, k_{bSn}, and k_{bTn}. A rate constant, k_{nn}, is introduced for excitation and bleaching pathways into even higher-excited states, which is possible in the case of two-photon excitation.

2.1. Exact Calculation of the Time-Dependent Populations for Pulsed Excitation

The time-dependent populations of each of the five levels are obtained by solving the rate equation system, given in Equations (3a–e), for known excitation and de-excitation rate constants over the time course of the irradiance (e.g., in pulsed excitation).[42,43]

$$\dot{S}_0(t) = -k_{01}S_0 + (k_f + k_{IC})S_1 + k_T T_1 \qquad (3a)$$

$$\dot{S}_1(t) = k_{01}S_0 - (k_0 + k_{1n} + k_{bS})S_1 + k_{n1}S_n \qquad (3b)$$

$$\dot{S}_n(t) = k_{1n}S_1 - (k_{n1} + k_{bSn})S_n \qquad (3c)$$

$$\dot{T}_1(t) = k_{ISC}S_1 - (k_T + k_{T1n} + k_{bT})T_1 + k_{Tn1}T_n \qquad (3d)$$

$$\dot{T}_n(t) = k_{T1n}T_1 - (k_{Tn1} + k_{bTn})T_n \qquad (3e)$$

Fast vibrational relaxation within the S_1 and T_1 manifold is assumed, that is, the instantaneous population of the lowest vibronic levels. Similarly, in the case of one-photon excitation at 350 nm and two-photon excitation at 800 nm, excitation into a singlet state higher in energy than S_1, $S_{>1}$ (e.g., second- or third-excited singlet state), relaxation to S_1 is assumed to occur on the sub-picosecond time scale. Therefore, with respect to subsequent processes, these $S_{>1}$ states are treated in the same way as the singlet excited state, S_1. This approximation is valid as long as other depopulation processes, such as intersystem crossing, de-excitation into S_0, bleaching, and excitation into higher electronic states, are slower than this sub-picosecond relaxation. However, at high-excitation irradiances, for example, with femtosecond pulses, the absorption into higher-excited states may compete with the relaxation process.

2.2. The Steady-State Approximation

The microscopic rate constants for photobleaching are much smaller than those for intramolecular relaxation. It is therefore justified to treat the kinetics of both processes separately.

In the steady-state approximation, the populations of the electronic state system described by the rate Equations (3a–e) are assumed to have reached the steady-state equilibrium within nanoseconds and microseconds in the case of singlet and triplet states, respectively. With $S_0(t) + S_1(t) + T_1(t) + S_n(t) +$

$T_n(t) = 1$, it is appropriate to use steady-state population probabilities,[43] given in Equations (4a–d):

$$S_{0eq} = k_{Tn1} k_{Sn1} k_T k_0 / X \tag{4a}$$

$$S_{1eq} = S_{0eq} k_{01} / k_0 \qquad T_{1eq} = S_{1eq} k_{ISC} / k_T \tag{4b}$$

$$S_{neq} = S_{1eq} k_{1n} / k_{Sn1} \qquad k\text{-}T_{neq} = T_{1eq} k_{T1n} / k_{Tn1} \tag{4c}$$

$$X = k_{Tn1}[k_T(k_{Sn1}(k_0 + k_{01}) + k_{01}k_{1n})] + (k_{T1n} + k_{Tn1})(k_{ISC}k_{Sn1}k_{01}) \tag{4d}$$

While the steady-state approximation is precise for cw excitation, it can be successfully applied in the case of pulsed excitation by assuming quasi-continuous, pulsed-averaged excitation irradiances. This provides a markedly simplified description, which circumvents solving the rate Equations (3a–d) over the pulse train. The rate constant for excitation [Eqs. (1) and (2)] has to be multiplied by the pulse gain factor, g_p,[35,36,74,75] described in Equation (5)

$$g_p = \frac{\int_{-\infty}^{+\infty} f_r [I(t)]^n dt}{\left[\int_{-\infty}^{+\infty} f_r I(t) dt\right]^n} \tag{5}$$

which takes the temporal pulse profile of the excitation irradiance, $I(t)$, and the repetition rate, f_r, of the laser pulses into account. For one-photon excitation ($n = 1$), g_p takes a value of unity and the rate of excitation, k_{01}, stays the same as given by Equation (1). In the case of two-photon excitation ($n = 2$), an approximated temporal sech^2 pulse profile with pulse width, τ_P, leads to $g_p = 0.588/(f_r\ \tau_P)$. For the present experimental conditions of two-photon excitation with $f_r = 76$ MHz and $\tau_P = 200$ fs, g_p takes a value of 38690.

Similar steady-state approximations have been used in previous studies using cw excitation in order to extract triplet[50] and photobleaching parameters[42,43] from FCS measurements, to optimize high-sensitivity fluorescence measurements,[77] to resolve the photobleaching kinetics of fluorescein[78] or Rh6G,[56,57] to describe the statistics in single-molecule fluorescence detection in solution[79,80] and in microdroplets,[53] and to investigate the bleaching characteristics of Rh6G in a film of polymethylacrylate (PMA).[55] In previous theories concerned with photobleaching of dye molecules under pulsed one- and two-photon excitation, time-dependent numerical calculations of populations over the time-course of a single excitation pulse were performed, resulting in effects such as pulse saturation.[54,65] Pulse saturation is provoked by the fact, that in one and the same molecule an excitation event, for example, $S_0 \rightarrow S_1$, can only be evoked once per pulse. This effect is not taken into account when constituting quasi-continuous excitation. The present study will disclose the limitation of the simplified model based on steady-state populations, but will also demonstrate that in most cases it sufficiently describes the photobleaching and fluorescence emission behavior of dye molecules under the conditions of cw and pulsed confocal and two-photon microscopy.

2.3. The Survival and Photobleaching Probabilities

In order to include photobleaching into the steady-state model, the probability of an excited fluorophore of being fluorescent after time, t, of quasi-continuous irradiance is introduced in Equation (6):

$$p_{survive}(t) = k_z \exp(-k_z t) \tag{6}$$

The bleaching reaction is assumed to be quasi-unimolecular with the effective pseudo-first-order bleaching rate constant, k_z,[42,43,63,77,81] expressed by microscopic photobleaching rate constants, [Eq. (7)]:

$$k_z = (k_{bS} S_{1eq} + k_{bT} T_{1eq} + k_{bSn} S_{neq} + k_{bTn} T_{neq}) = (k_b + k_{bn} I) S_{1eq} \tag{7}$$

with Equations (7a) and (7b)

$$k_b = k_{bS} + (k_{ISC}/k_T) k_{bT} \tag{7a}$$

$$k_{bn} = (k_{bXn}/k_{Xn1})(g_p^{qcw} \sigma_{1n} \gamma + (k_{ISC}/k_T) \sigma_{T1n} \gamma) \tag{7b}$$

The composite microscopic bleaching rate constants, k_b and k_{bn}, express the photobleaching reactivity from the first-excited, S_1 and T_1, and higher-excited electronic states, S_n and T_n, respectively. The rate constants, $k_{bXn} = k_{bSn} = k_{bTn}$ and $k_{Xn1} = k_{n1} = k_{Tn1}$, cannot be differentiated for singlet and triplet states, that is, mean parameters are obtained. Furthermore, a pulse enhancement factor, g_p^{qcw}, has to be introduced in the steady-state model to accommodate the fact that excitation is performed from a short-lived state (S_1, $S_{>1}$ or their higher vibronic states). Such excitation and subsequent bleaching is favored by the high photon flux densities of pulsed light.

In order to set a quantity to the reactivity, the probability of photobleaching, p_b, is introduced in Equation (8),[42,43]

$$p_b = \frac{k_z}{k_0 S_{1eq}} = \frac{(k_b + k_{bn} I) S_{1eq}}{k_0 S_{1eq}} = \frac{k_b}{k_0} + \frac{k_{bn}}{k_0} I \tag{8}$$

It is apparent that the populations of the S_n and T_n states open up new reaction channels, which introduce an additional irradiance dependency to the reactivity. For negligible populations of the S_n and T_n states, that is, $k_{1n} = k_{T1n} = 0$, $p_b = k_b/k_0$ represents a constant value.

2.4. The Fluorescence Brightness

The observation of single fluorescent molecules in a small open-volume element with a size of a few femtoliters by confocal microscopy allows to describe the fluorescence characteristic on the basis of a single fluorophore. An adequate measure for photophysical parameters is the fluorescence brightness, which is defined as the mean number of fluorescence photons, N_F, detected from a single fluorophore within the observation time, t_{ob}. The fluorescence brightness depends on the fluorescence detection efficiency, ψ_F, as well as on the probability to

be in the first-excited singlet state S_1, from where emission with a quantum yield, $\phi_F = k_f/k_0$, occurs.

For an exact solution using the populations, deduced from solving the rate Equations (3a–e) over the time-dependent excitation irradiance, N_F is given by the probabilities, $S_1(i)$, of being in the S_1 state after the ith excitation pulse, [Eq. (9)]

$$N_F = \sum_i^{n_P} \psi_F \phi_F S_1(i) \tag{9}$$

Photobleaching is included in Equations (3a–e) by the microscopic rate constants. The total number of pulses is given by the observation time and the pulse repetition rate, $n_P = t_{ob} f_r$. The values of $S_1(i)$ can be calculated by solving the rate Equations (3a–e) over the time course of irradiance, $I(t)$, given by the approximated temporal sech^2 pulse profile with pulse width, τ_p, and repetition rate, f_r.

For the simplified model of steady-state populations, N_F is directly proportional to S_{1eq}. According to Equation (6), photobleaching reactions limit the attainable time of fluorescence emission and, hence, reduce the mean number of fluorescence photons, [see Eq. (10)]

$$N_F = \psi_F k_F S_{1eq} \frac{1}{k_z} \int_0^{t_{ob}} p_{survive}(t) dt = \psi_F \frac{\phi_F}{p_b} [1 - \exp(-k_z t_{ob})] \tag{10}$$

In the case of freely diffusing fluorophores, the observation time is given by the mean transit time of a single fluorophore through the confocal detection volume, $t_{ob} = 4/3\tau_D$.[12] τ_D is the characteristic diffusion time, defined by the fluorescence correlation function as outlined below.

The spatial dependence of all irradiance-dependent rate constants (e.g., k_{01}, k_z) is given by the excitation–irradiance distribution in the focus, which is assumed to be a three-dimensional Gaussian profile, $I(x,y,z) = I_0 \exp(-2(x^2+y^2)/\omega_0^2) \exp(-2z^2/\omega_z^2)$ with the focal irradiance $I_0 = I(z=0)$ and $1/e^2$ radii ω_0 and ω_z in radial and axial directions, respectively. In the case of two-photon excitation, this profile is effectively squared. To simplify expressions for photophysical processes, it is justified to approximate the excitation volume by a cylindrical profile with radius ω_0 and $\omega_0/2^{1/4}$ for one- and two-photon excitation, respectively. Consequently, an average rate constant, $k(I_{av})$, can be defined. For one-photon excitation, I_{av} is given by $I_0/2$.[43,50] In the case of two-photon excitation, it has a value of $I_{av} = I_0/2^{1/2}$.[82]

2.5. Fluorescence Correlation Spectroscopy

Temporal fluctuations in the fluorescence signal about an average value, $F(t) = \langle F(t) \rangle + \delta F(t)$, arise from variation in the fluorescent dye concentration by diffusion or chemical reaction such as photobleaching. In fluorescence correlation spectroscopy (FCS), these fluctuations are analyzed by the second-order autocorrelation function, $G(t_c)$, shown in Equation (11):[17]

$$G(t_c) = 1 + \frac{\langle \delta F(t) \delta F(t + t_c) \rangle}{\langle F(t) \rangle^2} \tag{11}$$

Here, t_c represents the correlation time. Triangular brackets indicate averaging over the measurement time, t.

Besides diffusion of molecules in and out of the confocal detection volume, two photochemical reactions that lead to characteristic fluorescence fluctuations have to be taken into account: 1) triplet formation in a reversible photochemical equilibrium leads to bunched dark periods in fluorescence emission of a single dye molecule,[50] and 2) irreversible photobleaching reaction to a nonfluorescent product gives rise to an abrupt termination of fluorescence emission, thus resulting in an apparent shorter observation time.[43,51,54,65,67] Because the total sample volume is much larger than the excitation volume, the depletion of fluorophores within the focus due to photobleaching is balanced by a net in-flow from out-of-focus regions due to the concentration gradient formed. Consequently, photobleaching can be treated as a chemical pseudo-equilibrium reaction using the effective bleaching rate constant, $k_z(I_{av})$.

In this way, the autocorrelation function that takes diffusion dynamics, triplet and photobleaching kinetics into account can be approximated by Equation (12).[43,50,67] Compared to Equation (19) in ref. [43], the triplet term is added to the diffusion and bleaching term. The triplet kinetic can be treated separately, since this process is independent of diffusion and bleaching, which occurs on a much slower time scale [Eq. (12)]

$$G(t_c) = 1 + [(S-B)/S]^2 [G_D(t_c) G_B(t_c) + G_T(t_c)] \tag{12}$$

with Equations (12a–e)

$$G_D(t_c) = \frac{1}{N} \left(\frac{1}{1 + t_c/\tau_D} \right) \left(\frac{1}{1 + (\omega_0/\omega_z)^2 (t_c/\tau_D)} \right)^{1/2} \quad \text{(diffusion)} \tag{12a}$$

$$G_B(t_c) = 1 - A + A \exp(-k_z(I_{av}) t_c) \quad \text{(bleaching)} \tag{12b}$$

$$G_T(t_c) = \frac{T_{1eq}(I_{av})}{1 - T_{1eq}(I_{av})} \exp(-t_c/t_T(I_{av})) \quad \text{(triplet)} \tag{12c}$$

$$T_{1eq}(I_{av}) = k_{01}(I_{av}) k_{ISC} / (k_{01}(I_{av})(k_{ISC} + k_T) + k_T k_0) \tag{12d}$$

$$1/t_T(I_{av}) = k_T + (k_{01}(I_{av}) k_{ISC} / (k_{01}(I_{av}) + k_0)) \tag{12e}$$

The characteristic diffusion time is given via the diffusion coefficient, D, by $\tau_D = \omega_0^2/4D$ for one-photon excitation[50] and $\tau_D = \omega_0^2/8D$ for two-photon excitation.[67,75] N is the mean number of fluorescent molecules in the detection volume. $T_{1eq}(I_{av})$ denotes the equilibrium fraction of molecules in T_1 neglecting the population of higher-excited electronic states, S_n and T_n [$k_{1n} = k_{T1n} = 0$, compare Eq. (4)]. $t_T(I_{av})$ is the characteristic triplet correlation time, and A is an amplitude that describes the average bleaching decay with a rate constant, $k_z(I_{av})$. In the presence of significant background signal, B, contributing to the

total detected signal, S, the amplitude of the correlation function, $G(t_c=0)$, is corrected via the prefactor $[(S-B)/S]^2$.[83]

3. Results and Discussion

3.1. Photokinetic Constants of Rh6G in Water

The assignment of photokinetic constants to Rh6G is essential for the evaluation of our experimental results using the above-mentioned model. The one-photon absorption cross-section values, $\sigma_{01}(\lambda)$, at the applied wavelengths, λ, are obtained from the absorption spectrum of Rh6G in water (Figure 1b), and are listed in Table 1. The fluorescence lifetime, $\tau_0=(k_0)^{-1}=3.9$ ns, was determined by time-correlated single photon counting. With a quantum yield of $\phi_F\approx 0.95$,[84,85] the rate constant for deactivation by fluorescence amounts to $k_f=\phi_F/\tau_0=2.4\times 10^8\ s^{-1}$. The one-photon absorption cross-sections for the higher-excited states and the two-photon absorption cross-section at the applied wavelengths were taken from literature: $\sigma_{1n}(350\ nm)=2.5\times 10^{-16}\ cm^2$,[86] $\sigma_{1n}(515\ nm)=0.77\times 10^{-17}\ cm^2$ and $\sigma_{T1n}(515\ nm)=3.85\times 10^{-17}\ cm^2$,[49,87] and $\delta_{01}(800\ nm)=2\times 10^{-48}\ cm^4\,s$.[36,74] The lifetimes of the higher-excited states, $(k_{Sn1})^{-1}$ and $(k_{Tn1})^{-1}=200$ fs, were determined from the data at 515 nm excitation.[43]

A cell bleaching method at low continuous wave excitation irradiances ($I_0<10^3\ W\,cm^{-2}$) was used to determine solely the photobleaching parameters responsible for a reaction from the first-excited electronic states with high accuracy.[43,63] The photobleaching reactions from S_1 and T_1 cause an exponential decrease of the fluorescence intensity of a stirred Rh6G solution (concentration between 10^{-5} and 10^{-9} M) in a cuvette over illumination time [compare Eqs. (6) and (7)]. The characteristic time, thus, directly determines the microscopic bleaching rate constants, k_b, at the applied wavelengths, as listed in Table 1. Within the error limits of approximately 30% determined by multiple measurements,[42] the rate constants and probabilities of photobleaching, $k_b=795\ s^{-1}$ and $p_b=3.1\times 10^{-6}$ (at 350 nm) and $k_b=650\ s^{-1}$ and $p_b=2.5\times 10^{-6}$ (at 502 to 528 nm), were found to be independent of I_0 at these low excitation irradiances, that is, $I_0<10^3\ W\,cm^{-2}$. This is in agreement with the assumption that under these conditions excitation to S_n and T_n can be neglected [compare Eqs. (7) and (8)].[43] The photobleaching parameters, k_b and the lower limit of p_b, listed in Table 1 are of major interest in low power applications, such as in wide-field fluorescence imaging.

3.2. Continuous Wave and Picosecond-Pulsed Excitation into the S_1 State

3.2.1. Analysis of Single-Molecule Fluorescence Time Traces

The dependence of the mean number of detected fluorescence photons per single dye on the incident irradiance, $N_F(I_{av})$, as described by Equations (9) and (10), can be obtained from the direct observation of fluorescence bursts from single dye molecules diffusing through the focal volume at different irradiances (Figure 2a). One way to extract N_F from the raw single-molecule fluorescence signal traces in Figure 2a is simply counting the number of fluorescence photons per single burst where background photons have been subtracted. Thereby, the binning time is set close to the value of the transit time. An accurate value of N_F can be obtained by averaging over those bursts, which exhibit a number, $N_F>0.7\,N_{Fmax}$ (N_{Fmax}; maximum value of a measurement). Only those bursts are selected by this threshold criterion, which correspond to a transit of a single molecule through the center of the detection volume. In this way, N_F was in these experiments determined from fluorescence bursts collected for 60 seconds.

Figure 2b shows the values of N_F determined from the single-molecule time traces of Rh6G in aqueous solution for different continuous wave excitation irradiances at 515 nm. The extracted irradiance dependence of N_F includes three re-

Table 1. *Photophysical parameters of Rh6G in water and ethanol as indicated, extracted from the steady-state model.*

λ[a]	E_n[b]	σ_{01}[c–f] δ_{01}[g]	σ_{X1n}[h–i]	k_{ISC}[j]	k_T[j]	k_b[k–m]	k_{bXn}[n]	$p_b(I)$[o]	N_F[p]
350[q]	7.1	0.36[c]	25[h]	[t]	[t]	795[k]	6800	4–23 500	3
515[r]		1.35[d]							
cw	4.9	2.22[e]	0.77[h]	1.1	0.49	650[l]	28	3–50	540
pulsed 800[s]	4.9	2.70[f]	3.85[i]	1.1	0.38		28	3–50	540
water	4.7	2[g]	[t]	[t]	[t]	795[m]	0.02	785	30
ethanol	4.7	2[g]	[t]	[t]	[t]	795[m]	0.0064	255	230

[a] Applied wavelength [in nm]. [b] Energy content of S_n in eV. [c-f] Absorption cross-sections for one-photon excitation in $10^{-16}\ cm^2$ at 350[c], 502[d], 515[e], and 528 nm[f] determined from Figure 1b. [g] Absorption cross-sections for two-photon excitation in $10^{-48}\ cm^4\,s$ taken from refs. [36,74]. [h–i] Absorption cross-sections for excitation into S_n[h] or T_n[i] in $10^{-17}\ cm^2$ taken from refs. [49,86,87]. [j] Rate constant for triplet intersystem crossing, k_{ISC}, and de-excitation, k_T, in $10^6\ s^{-1}$ from FCS analysis (Figure 3). [k–m] Composite microscopic rate constants $k_b=k_{bS}+(k_{ISC}/k_T)k_{bT}$ for bleaching from the first-excited states, S_1 and T_1 [Eq. (7)] in s^{-1} determined from cell bleaching experiments at 365[k] and 502 to 528 nm[l], and for two-photon excitation assumed as that of 365 nm.[m] [n] Rate constant for bleaching from higher-excited states, X_n (X = S or T), in $10^7\ s^{-1}$ not distinguishable for S_n or T_n (including a pulse enhancement factor for 350 and 800-nm excitation). [o] The probability of photobleaching in 10^{-6} [Eq. (8)]; one-photon excitation: due to the dependence on irradiance, I [Eq. (8)], a range is given including irradiances from $I_{av}=10^3$ to $10^6\ W\,cm^{-2}$; two-photon excitation: constant due to saturation of the transition to S_n [Eq. (13)]. [p] Maximum number of detected photons from Figures 2b, 4b and 6 normalized onto an observation time of $t_{ob}=0.5$ ms. [q] Femtosecond-pulsed excitation. [r] Continuous wave (cw) or picosecond-pulsed excitation at 502, 515, or 528 nm. [s] Femtosecond-pulsed two-photon excitation in water or ethanol. [t] Not determinable or observable.

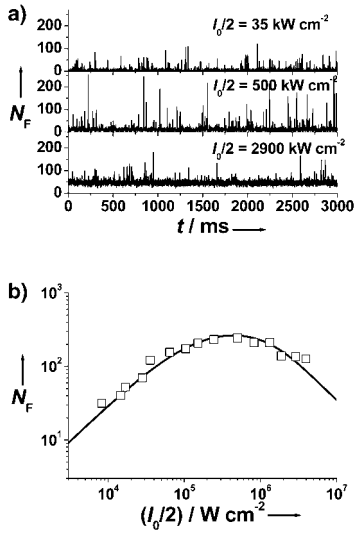

Figure 2. *a) Time traces of the number of photon counts, $N_\#$, detected within consecutive intervals of 0.5 ms bin width for a single-molecule Rh6G sample (water, ≈5 pM, cw excitation at 515 nm, $\tau_D = 0.18$ ms, $\omega_0 = 0.46$ μm) at three different excitation irradiances, $I_0/2$. b) Dependence of the mean number of detected fluorescence photons from a single fluorophore, N_F (open squares), on the excitation irradiances, $I_0/2$, as extracted from the traces of (a) and its simulation (black line) using Equation (10) with the following parameters, $\psi_F = 2\%$, $t_{ob} = 0.24$ ms, $k_0 = 2.56\times10^8\ s^{-1}$, $k_f = 2.4\times10^8\ s^{-1}$, $\sigma_{01} = 2.22\times10^{-16}\ cm^2$, $k_{ISC} = 1.1\times10^6\ s^{-1}$, $k_T = 4.9\times10^5\ s^{-1}$, $\sigma_{1n} = 0.77\times10^{-17}\ cm^2$, $\sigma_{T1n} = 3.85\times10^{-17}\ cm^2$, $k_b = 650\ s^{-1}$, $(k_{Sn1})^{-1} = (k_{Tn1})^{-1} = 200$ fs, and $k_{bSn} = k_{bTn} = 2.8\times10^8\ s^{-1}$.*

gimes: 1) a linear dependence for low irradiances ($k_{01} \ll k_0$), as measured in the cell bleaching experiments, 2) a saturation to a maximum value due to triplet population and photobleaching, and 3) a decrease for high irradiances, that is, $I_{av} = I_0/2 > 10^6$ W cm^{-2}, which can only be described by photobleaching from higher-excited states, S_n and T_n. The minimal theoretical model required to satisfactorily describe the experimental observation of $N_F(I_{av})$ in Figure 2b is an electronic five-level system shown in Figure 1a that takes a two-step photolysis from the higher-excited states, S_n and T_n, into account.[42,43,51,54,55,57,63,65,67,68,70,72,80] The theoretical prediction based on the simplified steady-state model of Equation (10) and photophysical parameters known from previous measurements,[42,43] also shown in Figure 2b, is in good agreement with the experimental data.

3.2.2. Analysis of FCS Measurements

An independent determination of photoblaching parameters and/or the $N_F(I_{av})$ dependence is provided by fluorescence correlation spectroscopy (FCS) measurements taken at different irradiances using the same experimental set up and excitation conditions. The initial FCS amplitudes that give the mean number, N, of fluorescent molecules in the detection volume and the mean transit time, t_{ob} [compare Eq. (2)], allow the calculation of $N_F = t_{ob}\ (S-B)/N$ from the signal, S, and the background, B, which in principle yields the same values as obtained by the single-molecule time traces of Figure 2. However, FCS directly yields information about triplet and photobleaching kinetics, thus, providing a better understanding of the underlying photokinetic processes leading to the observed irradiance dependence.

Figure 3 presents such exemplary FCS data, $G(t_c)$, and their analysis for cw and pulsed excitation at 502 nm. A higher irradiance has two effects on $G(t_c)$: 1) Due to a more efficient excitation, the triplet state is more populated, resulting in an additional exponential decay on the microsecond time scale.[50] 2) Photobleaching becomes evident by an apparently reduced diffusion (or observation) time.[42,43,51,54,65,67] The photophysical and diffusion parameters are extracted by fitting Equation (12) to the measured FCS curves. First, data at low excitation irradiances ($I_0 < 10^5$ W cm^{-2}) are recorded where both triplet and photobleaching effects can be neglected ($A = T_{1eq} = 0$). The parameters of diffusion, τ_D, and of the detection volume, ω_0 and ω_z, are determined by assuming a diffusion coefficient of $D = 3\times10^{-6}$ cm^2 s^{-1} for Rh6G in water.[88] In a second step, these

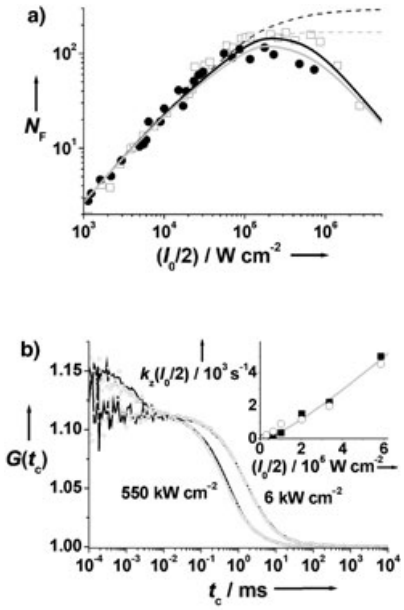

Figure 3. *a) Dependence of the mean number of detected fluorescence photons from a single fluorophore, $N_\#$ on the quasi-continuous excitation irradiances, $I_0/2$, as extracted from FCS measurements of Rh6G (10^{-9} M in water) for cw (open squares) and picosecond-pulsed excitation (black dots) at 528 nm ($\tau_D = 0.18$ ms, $\omega_0 = 0.46$ μm). The corresponding simulated dependences are based on the simplified steady-state model of Equation (10) (black lines) and the exact calculation of the rate equations over the pulse train [Eq. (9), grey lines] with the following parameters, $\psi_F = 2\%$, $t_{ob} = 0.24$ ms, $k_0 = 2.56\times10^8\ s^{-1}$, $k_f = 2.4\times10^8\ s^{-1}$, $\sigma_{01} = 2.7\times10^{-16}\ cm^2$, $k_{ISC} = 1.1\times10^6\ s^{-1}$, $k_T = 4.9\times10^5\ s^{-1}$, $\sigma_{1n} = 0.77\times10^{-17}\ cm^2$, $\sigma_{T1n} = 3.85\times10^{-17}\ cm^2$, $k_b = 650\ s^{-1}$, $(k_{Sn1})^{-1} = (k_{Tn1})^{-1} = 200$ fs, and $k_{bSn} = k_{bTn} = 2.8\times10^8\ s^{-1}$. The dashed lines represent the simulated data without any bleaching reaction ($k_b = k_{bSn} = k_{bTn} = 0$). b) Normalized fluorescence autocorrelation curves, $G(t_c)$, of Rh6G (10^{-9} M in water) for two different excitation irradiances, $I_0/2$, with cw (black line) and picosecond-pulsed excitation (open dots) at 502 nm ($\tau_D = 0.18$ ms, $\omega_0 = 0.46$ μm). Inset: Irradiance dependence of the effective bleaching rate constant, $k_z(I_0/2)$, determined from the measured autocorrelation curves in (b) using Equation (12) for cw (black squares) and pulsed (open dots) excitation. Both curves are well described by Equation (7) (grey line) using the following parameters, $k_0 = 2.56\times10^8\ s^{-1}$, $\sigma_{01} = 1.35\times10^{-16}\ cm^2$, $k_{ISC} = 1.1\times10^6\ s^{-1}$, $k_T = 4.9\times10^5\ s^{-1}$, $\sigma_{1n} = 0.77\times10^{-17}\ cm^2$, $\sigma_{T1n} = 3.85\times10^{-17}\ cm^2$, $k_b = 650\ s^{-1}$, $(k_{Sn1})^{-1} = (k_{Tn1})^{-1} = 200$ fs, and $k_{bSn} = k_{bTn} = 2.8\times10^8\ s^{-1}$.*

values are fixed within the fits to the correlation curves at higher irradiances, resulting in values for $k_z(I_{av})$, $T_{1eq}(I_{av})$, and $t_T(I_{av})$.

$T_{1eq}(I_{av})$ and $t_T(I_{av})$ directly specify the rate constants for triplet intersystem crossing, $k_{ISC}=(1+(k_f+k_{IC})/k_{01})T_{1eq}(I_{av})/t_T(I_{av})$ and $k_T=(1-T_{1eq}(I_{av}))/t_T(I_{av})$,[50] which only requires the knowledge of σ_{01} or δ_{01}, k_0 and I_{av}. Such a procedure has been previously presented in detail.[50,82] As an example, the analysis of FCS curves upon cw excitation at 515 nm results in values listed in Table 1, which coincide well with literature data.[50,82]

The dependence of the effective photobleaching rate, $k_z(I_{av})$, on the irradiance can by knowledge of σ_{01} or δ_{01}, k_0, σ_{1n} and σ_{T1n}, and I_{av} be well-described by Equation (7) (inset of Figure 3b). Accordingly, the fit yields the photophysical parameters of the higher-excited states, k_{bXn} and k_{Xn1}, whereby singlet, X=S, and triplet states, X=T, cannot be distinguished. Only mean rate constants can be obtained.

The FCS analysis constitutes two simplifying assumptions: 1) The observed parameters, $k_z(I_{av})$, $T_{1eq}(I_{av})$, and $t_T(I_{av})$, are theoretically described using the model based on steady-state populations. 2) A more important approximation is the neglect of saturation of S_1 and T_1 populations. This leads to an inappropriate weighting of the signal in the FCS curve at high irradiances, as has been discussed in previous reports.[50,89–92] In particular, saturation leads to an apparent increase of the diffusion time, τ_D, which is overwhelmed by the decrease in τ_D caused by the photobleaching reaction. Another consequence of saturation might be the limited applicability of the space-averaged irradiance, I_{av}, since the saturation is less pronounced at the periphery of the three-dimensional approximated focal irradiance profile. It is beyond the scope of this work to perform a space-dependent simulation as, for example, has been reported by Widengren et al.[50] and Enderlein and co-workers.[91,92] As our results show, the above approximations describe the irradiance dependency of the fluorescence, $N_F(I)$ (e.g., Figure 2b), in an acceptable and efficient manner.

3.2.3. Comparison of Continuous Wave and Picosecond-Pulsed Excitation

An important question arises, whether pulsed excitation into the S_1 state as required for time-resolved fluorescence microscopy leads to a reduced fluorescence signal when compared to cw excitation. Because of the high photon density applied within the pulse peak, an enhanced two-step excitation into higher-excited states may be expected.[54,65,93–95] In this experiment, we use a train of picosecond pulses (pulse duration of 180 ps at a repetition rate, $f_r=73$ MHz, which is commonly employed in time-resolved single-molecule fluorescence experiments[2,30]). Figure 3a shows the irradiance dependence of N_F for both pulsed and cw excitation, as determined from the amplitude of the corresponding FCS data. A difference in maximum achievable fluorescence photon counts of a factor of 1.5 is observed, which favors cw excitation.

The comparison of FCS curves upon pulsed and cw excitation in Figure 3b reveals no difference in the photobleaching rate constants (compare Table 1). This important observation indicates that most two-step photolysis reactions have to occur via the triplet state. Its population with a lifetime >1 μs, in contrast to the singlet state with a lifetime <4 ns, is still present for the next pulse. Hence, the probability of absorbing an additional photon is independent of the "dark" period of about 13.7 ns in between two consecutive laser pulses. This fact is supported by the five times higher absorption cross-section for excitation into T_n, $\sigma_{T1n}=3.85\times10^{-17}$ cm^2 compared to $\sigma_{1n}=0.77\times10^{-17}$ cm^2 as measured by Thiel.[49,87] When exciting at the main absorption peak (S_1), the higher-excited triplet state, T_n, has previously been identified as the main bleaching pathway for two-step photolysis.[55,63,67,80] This bleaching mechanism is well influenced by oxygen and radical scavengers such as ascorbid acid,[42,67] which underlines the formation of a radical ion pair as well as the influence of oxygen on the triplet photobleaching.

Both theoretical models, the exact calculations over the pulse train of irradiance [Eq. (9)] and the steady-state approximation [Eq. (10)], describe well data observed for both pulsed and cw excitation using the same set of parameters. A pulse enhancement factor, g_p^{qcw} [Eq. (7)], does not have to be established, in as much as photobleaching mainly occurs via the rather long-lived triplet state. This result supports the previous conclusion that no additional photobleaching reaction pathway needs to be introduced for one-photon excitation into the S_1 state with picosecond pulses.

Therefore, the slightly lower maximum achievable photon counts for pulsed excitation is attributed to pulse saturation. Compared to cw excitation, the increased pulse peak irradiance leads to a pronounced degree of saturation of the optical S_0–S_1 transition. For cw excitation, a single fluorophore in its ground state can be excited at any time. In the case of pulsed excitation, absorption can only occur during a fraction of time, that is, during the pulse. This disadvantage is not compensated by the enhanced peak irradiance, since a fluorophore is only excited once per pulse. Pulse saturation becomes more obvious when theoretically comparing the achievable photon counts in the absence of photobleaching reactions present (dashed lines in Figure 3a). This results in a 1.5 times higher achievable number of fluorescence photons for cw excitation. This comparison is in accordance to previous results obtained from rate theory,[92] and also highlights the sole discrepancy introduced when applying the quasi-continuous steady-state approximation for pulsed excitation.

Analogous effects are observed at 502, 515 and 528-nm excitation, yielding rate constants similar to those presented in Table 1 for 515-nm excitation. Consequently, shifting the wavelength of cw excitation within the main absorption peak of the lowest-excited singlet state, S_1 (500 to 530 nm, Figure 1b), cannot overcome the limitations imposed by the two-step photolysis and has no significant influence on the fluorescence brightness of a single Rh6G molecule at high irradiances. On the basis of these results, it has been discussed how the fluorescence yield can be optimized by different focal diameter, that is, by different observation or transit times of a single fluorophore, resembling a trade-off between maximum achievable N_F and decreased signal-to-background ratio.[42,43]

In conclusion, the use of picosecond pulses at a megahertz repetition rate is of no disadvantage in terms of photobleaching for confocal fluorescence microscopy and time-resolved fluorescence techniques, such as fluorescence lifetime imaging[23,25,26] and multi-parameter fluorescence detection (MFD).[2,30] However, shorter pulses (e.g., sub-picosecond pulses), especially with excitation into higher singlet states, $S_{>1}$, will introduce a pulse enhancement factor, g_p^{qcw} [compare Eq. (7)], and, thus, an enhanced two-step photolysis, as will be discussed below. Furthermore, the maximum available fluorescence signal will be slightly lower for pulsed than for cw excitation due to a lower degree of saturation of the optical transition upon cw excitation, as can be concluded from rate theory. For a given quasi-continuous excitation irradiance, the pulse saturation effect will be more pronounced for lower laser repetition rates and shorter fluorescence lifetimes.

3.3 Two-Photon Femtosecond-Pulsed Excitation at 800 nm into Higher-Excited Singlet States

3.3.1. Analysis of Single-Molecule Fluorescence Time Traces

Two-photon excitation usually necessitates high photon flux densities, provided by high peak irradiances of femtosecond pulses [Eqs. (2) and (5)].[1,36] In this study, femtosecond pulses at 800 nm were applied, which predominantly lead to the direct excitation into the second-excited electronic singlet state, $S_{>1}$, higher in energy than the S_1 state. Figure 4a depicts fluorescence bursts from single fluorophores diffusing through the focal volume at two different irradiances. Figure 4b shows the dependence of the number of detected fluorescence photons, N_F, on the applied quasi-continuous irradiance, $I_{av} = I_0/2^{1/2}$, as observed from fluorescence bursts of single fluorophores. In contrast to the data obtained for one-photon excitation (compare Figures 2b and 3a), the dependence at lower excitation irradiances is not linear any more but exhibits a slope of two, confirming a two-photon excitation process.[1,35,36] The curve saturates and stays constant towards higher irradiances. The latter observation is in contrast to the one-photon excitation case. On the first glance, this would suggest an underlying simple three-state model involving the S_0, S_1 and T_1 states, without any population of higher-excited states. However, solely triplet population and photobleaching from first-excited electronic states cannot explain the low maximum number of observed photons, $N_F = 35$ within an observation time of $t_{ob} =$ 0.58 ms (compare $N_F = 300$ within $t_{ob} = 0.24$ ms in Figure 2b), which is an order of magnitude smaller than for one-photon excitation.

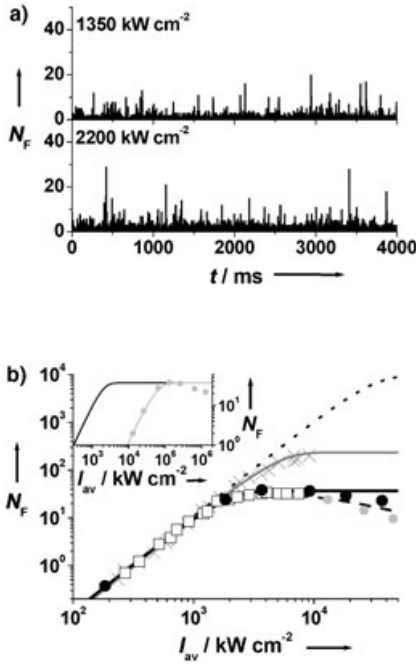

Figure 4. *a) Time traces of the number of photon counts, $N_\sharp$ detected within consecutive intervals of 1 ms bin width for a single-molecule Rh6G sample ($\approx$1 pM in water, femtosecond-pulsed excitation at 800 nm, $\tau_D = 0.44$ ms, $\omega_0 = 1.0\ \mu m$) at two different two-photon excitation irradiances, $I_{av} = I_0/2^{0.5}$. b) Dependence of the mean number of detected fluorescence photons from a single fluorophore, $N_\sharp$ on the excitation irradiances, $I_{av} = I_0/2^{0.5}$, as extracted from the traces of (a) (open squares) and from analogous single-molecule measurements of Rh6G in ethanol (grey crosses). The simulated dependences are based on the simplified steady-state model of Equation (10) (lines) and on the exact calculation of the rate equations over the pulse train [Eq. (9), black dots] with the following parameters, $\psi_F = 2\%$, $t_{ob} = 0.58$ ms (water) and 0.5 ms (ethanol), $k_0 = 2.56\times10^8\ s^{-1}$, $k_f = 2.4\times10^8\ s^{-1}$, $\delta_{01} = 2\times10^{-48}\ cm^4 s$, $g_p = 38\,690$, $k_{ISC} = 1.1\times10^6\ s^{-1}$, $k_T = 4.9\times10^5\ s^{-1}$, $k_b = 795\ s^{-1}$, and $k_{bSn} = 2\times10^5\ s^{-1}$ (water) and $6.4\times10^4\ s^{-1}$ (ethanol) for the simplified and $k_{bSn} = 7\times10^9\ s^{-1}$ (water) for the exact model. In addition, simulations without bleaching from higher-excited electronic states, S_n ($k_{bSn}=0$) (black dotted line), and with the possibility of excitation from S_n into even higher-excited electronic states with concurrent photobleaching, k_{nn} [Eq. (14)] (dashed line and grey dots, respectively, with $\sigma_{nn} = 1\times10^{-21}\ cm^2$ and $g_p^{qcw} = 1.8$), are shown. Inset: Simulated dependence of the mean number of detected fluorescence photons from a single Rh6G fluorophore in water, $N_\sharp$ on the two-photon excitation irradiance, $I_{av} = I_0/2^{0.5}$, at 800 nm using 200 fs (black line simplified steady-state model, same data as in the main figure) and 180 ps pulses (grey line simplified steady-state model and grey dots exact model). The constituted parameters are the same as in the main Figure but $k_{bSn} = 8\times10^6\ s^{-1}$ for the exact model.*

3.3.2. Analysis of FCS Measurements

In order to clarify the underlying saturation effect, FCS measurements were performed. Figure 5a shows the measured autocorrelation curves for three different quasi-continuous irradiances, $I_{av} = I_0/2^{1/2}$. As has been observed in previous two-photon excitation experiments,[65,67] triplet formation was found to be negligible. Furthermore, a remarkable decrease of the diffusion time is observed that is manifested by the shift of the curves towards smaller correlation times similar to that observed in Figure 3b. One might think of an increase in mobility due to local heating of the sample induced by the high irradiances applied.[73,93,94] However, theoretical calculations as well as experiments have shown, that this is unlikely to be the case in aqueous solutions.[65,67,96] The inset of Figure 5a shows the time course of the detected fluorescence signal after starting illumination. While the fluorescence count rate stays constant for low irradiances (upper graph), high irradiances give rise to an initial drop in the fluorescence signal (lower graph). This drop can be assigned to an instantaneous decrement in focal fluorophore concentration, which is balanced by the diffusion-

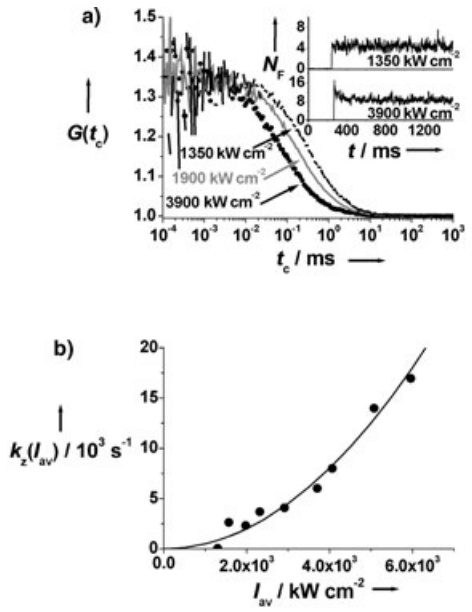

Figure 5. *a) Normalized fluorescence autocorrelation curves, G(t_c), of Rh6G (10^{-8} M in water, $\tau_D = 0.44$ ms, $\omega_0 = 1.0$ μm) for three different excitation irradiances, $I_{av} = I_0/2^{0.5}$, with femtosecond-pulsed two-photon excitation at 800 nm. Inset: Time course of the detected fluorescence signal for low and high irradiances (upper graph: $I_{av} = 1350$ kW cm^{-2}, lower graph: $I_{av} = 3900$ kW cm^{-2}). b) Irradiance dependence of the effective bleaching rate constant, $k_z(I_{av})$, determined from the measured autocorrelation curves in (a) using Equation (12) (black dots). The data are well-described by Equation (7) (black line) using the following parameters, $k_0 = 2.56 \times 10^8$ s^{-1}, $\delta_{01} = 2 \times 10^{-48}$ cm^4 s, $g_p = 38\,690$, $k_b = 795$ s^{-1}, and $k_{bSn} = 2 \times 10^5$ s^{-1}.*

controlled net in-flow of intact fluorophores until an equilibrium between photobleaching out-flow and in-flow is reached.[42,54,65,67] Thus, the apparent decrease of diffusion time is due to photobleaching and can be fitted by Equation (12). Figure 5b plots the values of the effective photobleaching rate as a function of irradiance, $k_z(I_{av})$, as obtained from the fit results. The irradiance dependence, $k_z(I_{av})$, is quadratic, which for the two-photon excitation can only be understood by a high reactivity from the $S_{>1}(400)$ state. Comparing Equation (7), $k_z = (k_b + k_{bn} I_{av}) S_{1eq}$, with $S_{1eq} \propto I_{av}^2$, excitation to higher-excited states would impose a dependence of higher order than quadratic. A fit of Equation (7) to the data neglecting photolysis from S_n ($k_{bn} = 0$) results in $k_b = 2 \times 10^5$ s^{-1}, which exceeds the corresponding value obtained from cell bleaching experiments at 365 nm ($k_b = 795$ s^{-1}) by a factor of ≈250. Due to this marked discrepancy, a process other than direct photobleaching from S_1 and $S_{>1}$ has to be responsible for the observed photobleaching reaction.

3.3.3. Saturation of Excited Singlet-State Absorption

Mertz[54] and Niesner et al.[65] proposed an efficient excitation process to higher electronic states, S_n, that successfully competes with the population of the first-excited electronic states, such as the triplet state. At high irradiances, every excitation into S_1 is immediately followed by the absorption of a third photon, thus leading to photobleaching reactions from S_n. Such a scenario is rendered by defining a quantum yield, $\phi_{1n} = k_{1n}/(k_0 + k_{1n})$, for the transition from S_1 or $S_{>1}$ to S_n. Within the irradiance dependence of k_z accessible by our FCS measurements (Figure 5b), the absorption into S_n dominates any other photophysical process, that is, $\phi_{1n} \approx 1$. This saturated behavior eliminates the irradiance dependence of the photobleaching step from S_n, $k_{bn} I \approx \phi_{1n} k_{bSn}$ [compare Eq. (7)]. Furthermore, in the absence of a significant triplet population, the saturation of the S_1 or $S_{>1}$ population can be neglected, that is, the rate constant for de-excitation, k_0, exceeds that of excitation, k_{01} [$k_{01}(\max, I_{av} = 10^4\ \text{kW cm}^{-2}) = 6.3 \times 10^6\ \text{s}^{-1}$, Eq. (2)], and $S_{1eq} \approx k_{01}/k_0$. The effective rate constant for photobleaching, k_z [Eq. (7)] can thus be simplified [$k_{01} \propto I_{av}^2$ for two-photon excitation; see Eq. (13)]

$$k_z = (k_b + \phi_{1n} k_{bSn})\, k_{01}/k_0 \propto {I_{av}}^2 \qquad (13)$$

In this way, the probability of photobleaching, $p_b = (k_b + k_{bSn})/k_0$ [Eq. (8)], becomes independent on the irradiance. As a result, the fluorescence yield, N_F [Eq. (10)], saturates but does not decrease with increasing I_{av}. This is depicted in Figure 4b, where the observed fluorescence yield is remarkably well-described by the approximated steady-state model [Eq. (10)], applying $k_{bSn} = 2 \times 10^5$ s^{-1} (black line). Similar results have also been demonstrated by Niesner et al.[65] using the exact numerical photophysical solution. The simulation of our experiment using the exact solution of the rate equations over the excitation pulse train [Eq. (9)] is also shown in Figure 4b (black dots). Compared to the simplified model based on steady-state populations, we have to constitute a 38 690 times higher bleaching rate, $k_{bSn} = 7.7 \times 10^9$ s^{-1}, to match the experimental data. This factor coincides with the applied pulse gain factor for two-photon excitation, $g_P = 38\,690$ [Eq. (5)], and originates from the fact that a saturated transition is assumed within the rate equations (i.e., $\phi_{1n} \approx 1$). As a consequence, no discrepancy arises between the two models within the range of irradiances applied, since no pulse saturation of the S_0–S_1 transition is present. However, at even higher irradiances ($> 10^4$ kW cm^{-2}), a decrease in N_F is predicted, which is caused by pulse saturation and cannot be explained by the simplified steady-state model. Such a prediction is supported by previous experimental observation, reporting a drop in fluorescence signal at high irradiances ($> 10^4$ kW cm^{-2}).[63,67,72,75]

In conclusion, this analysis confirms that the pulsed irradiances necessary for an efficient two-photon excitation lead predominantly to transitions into higher-excited states with severe photobleaching reactivity. The maximum achievable fluorescence yield does not exceed 35 photons for the present observation time and detection efficiency of about 0.58 ms and 2%, respectively. Thus, efficient single-fluorophore experiments and analyses are hard to accomplish, as observed previously.[72,75,97] Additional supporting evidence for the above photobleaching mechanism comes from the fact that in the case of Rh6G dissolved in ethanol the saturation of the fluorescence yield levels off at much higher irradiances, enabling the detection of up to 230 photons from a single molecule within an observation time of $t_{ob} = 0.5$ ms (crosses in Figure 4b). The suppression in

photobleaching reactivity from S_n, k_{bSn}, by an order of magnitude (Table 1) is based on the lower polarity of ethanol, which results in a reduced solvation energy of the electron–cation pair, leading to a lower dissociation probability. This effect has well been shown by constituting selective radical scavengers such as ascorbic acid.[67] Furthermore, in comparison to aqueous solutions differences in the two-photon photobleaching yield of dyes in different environments, such as on glass surfaces,[69,70] embedded in proteins or spheres,[72] lipid membranes[71] and living cells,[68] or at different temperatures,[73] have been observed, suggesting the strong dependence of higher-excited state reactivity on the environmental conditions, that is, polarity and temperature.

The simulation based on pulsed two-photon excitation using a 180-picosecond pulse width at 800 nm implying the same kinetic constants does not predict an increased number of achievable photons, N_F (inset Figure 4b). The longer pulse length only leads to a saturated behavior at higher irradiances, a fact that has been previously predicted by Niesner et al.[65]

3.3.4. Higher-Order Dependence of the Photobleaching Reaction

Within the experimental capabilities, we cannot unambiguously establish, whether the transition to the higher-excited singlet state, S_n, follows a one- or two-photon process. The saturated excitation into S_n necessitates $k_{1n} \gg k_0$, which is reasonably satisfied for $k_{1n} > 10^{10}\ s^{-1}$. Due to the high photon flux densities applied, a pulse enhancement factor, g_p^{qcw} [compare Eq. (7)], has to be introduced for this second absorption step from a picosecond to nanosecond lifetime-limited state [for two-photon excitation in addition to the intrinsic two-photon gain factor, $g_p = 38\,650$; see Eq. (5)]. This fact follows from our approximation of quasi-continuous irradiances. For the irradiances applied, $I_{av} \approx 10^6$ to $10^7\ W\,cm^{-2}$, and an assumed absorption cross-section of $\sigma_{1n} \approx 10^{-16}\ cm^2$ for one-photon ($k_{1n} = g_p^{qcw}\sigma_{1n}\gamma I_{av}$) or $\delta_{1n} \approx 10^{-49}\ cm^4\,s$[36,74] for two-photon excitation ($k_{1n} = g_p^{qcw} g_p(\delta_{1n}/2)\gamma^2 I_{av}^2$), g_p^{qcw} has to take a value of about 100 and 10^{33}, respectively. Compared to $g_p = 38\,650$ for the intrinsic two-photon process, it would be too high for a subsequent two-photon excitation process, but is within a reasonable range for subsequent one-photon excitation. The excited state absorption process occurs from a real state within its nanosecond (S_1) or picosecond ($S_{>1}$) lifetimes [compare Eq. (7)]. Therefore, the excitation process is most probably due to a one-photon excitation. The fluorescence yield in two-photon induced fluorescence is limited by a "three-photon" photolysis.

Several previous two-photon bleaching experiments have reported a similar dependence of the photobleaching reactivity on the third-order of irradiance.[64,65,67] However, other observations confirm an even higher dependency on up to the 4th and 5th order of the irradiance.[64,68] The possibility of simultaneous two-photon excited state absorption into higher-excited singlet states can be excluded, as has been discussed before. To a limited degree, the predicted fluorescence drop due to pulse saturation (black dots in Figure 4b) can account for an order higher than three. However, the pronounced irradiance dependence of an order higher than three requires the possibility of absorption from S_n to even higher-excited states and subsequent absorption steps. This possibility of multi-step excitation is indicated in Figure 1a by the kinetic rate constant, k_{nn}, leading to electronic states that are more reactive because of their energetic proximity to the ionization level at conditions of high irradiances. Since this transition is not saturated, we can extend our two-photon bleaching model of Equation (13) for high irradiances, by assuming $k_{nn}(1) = \sigma_{nn}\gamma I_{av}$ for one additional excitation step with the absorption cross-section, σ_{nn}. In a more general term, k_{nn} can be regarded as a multistep excitation, whereby $k_{nn}^*(m)$ combines the cross-sections of all m excitation steps following S_n [Eqs. (14a) and (14b)]

$$k_{nn} = \sum_{i=1}^{m} k_{nn}^*(i) I_{av}{}^i \qquad (m \geq 1) \tag{14a}$$

$$k_z = (k_b + k_{Sbn} + k_{nn})k_{01}/k_0 = \sum_{i=0}^{m} B_i I_{av}{}^{2+m} \tag{14b}$$

This polynomial model with prefactors, B_i, takes any order of bleaching into account. For $m = 0$, Equations (14a) and (14b) turn into the previously discussed case of Equation (13). The consequence of additional bleaching steps is the more pronounced drop in fluorescence towards high irradiances ($> 10^4\ kW\,cm^{-2}$), as exemplified in Figure 4b (dashed line or grey dots). The simplified model of steady-state population slightly underestimates this effect due to the onset of pulse saturation at these irradiances and has to introduce a pulse enhancement factor of $g_p^{qcw} \approx 1.8$ for the higher excitation steps [compare Eq. (7)].

Although in our case, the lack of data points towards high irradiances, which were not accessible due to the onset of other nonlinear processes,[63,75] does not provide a more accurate picture, it proves that all potential two-photon photobleaching mechanisms are accessible by this simple theoretical approach. The different behavior of the fluorescence yield towards high irradiances observed by Dittrich et al.[67] and others[64,68,72] prove that these multi-step photolysis processes are highly dependent on the dye itself, on its environment, and on additives.

3.4. One-Photon Femtosecond-Pulsed Excitation at 350 nm into Higher-Excited Singlet States

In order to directly compare the photobleaching mechanism found for two-photon excitation with that upon one-photon excitation into the same manifold of higher-excited singlet states, the above-mentioned experiments have been repeated with direct one-photon excitation to the higher-excited electronic singlet state, $S_{>1}(350)$, with femtosecond pulses at 350 nm (see absorption spectrum of Rh6G in Figure 1b).

Figure 6 shows the dependence of the mean number of detected photons, $N_F(I_{av})$, on the applied quasi-continuous irradiance, $I_{av} = I_0/2$, as determined from the FCS data (inset). Once more, one can recognize the three typical regimes, that is, the linear dependency at low irradiances, the saturation, and the

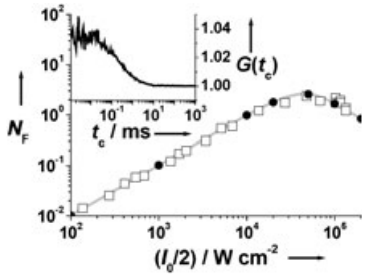

Figure 6. *Dependence of the mean number of detected fluorescence photons from a single fluorophore, N_F (open squares), on the excitation irradiances, $I_0/2$, as extracted from the fluorescence autocorrelation curves, $G(t_c)$ [Eq. (12)], of Rh6G (5×10^{-8} M in water, $\tau_D = 0.31$ ms, $\omega_0 = 0.6$ μm) for femtosecond-pulsed one-photon excitation at 350 nm. For illustration, an exemplary autocorrelation curve recorded at $I_0/2 = 48$ kW cm^{-2} is shown in the inset. The curve, $N_F(I_0/2)$, is well-described by the simplified steady-state model of Equation (10) (grey line) and by the exact calculation of the rate equations over the pulse train [Eq. (9), black dots] using the following parameters, $\psi_F = 0.4$ %, $t_{ob} = 0.41$ ms, $k_0 = 2.56\times10^8$ s^{-1}, $k_f = 2.4\times10^8$ s^{-1}, $\sigma_{01} = 3.6\times10^{-17}$ cm^2, $k_{ISC} = 1.1\times10^6$ s^{-1}, $k_T = 4.9\times10^5$ s^{-1}, $k_b = 795$ s^{-1}, $\sigma_{1n} = 2.5\times10^{-16}$ cm^2, $k_{n1} = (200\ fs)^{-1}$, $k_{bSn} = 3.75\times10^{10}$ s^{-1}, and $g_p^{qcw} = 1.8$.*

decrease at higher irradiances. When comparing the data with those of excitation around 515 nm (Figures 2 and 3), it is important to realize that the decrease of fluorescence yield already starts at one order of magnitude lower irradiances (10^4 compared to 10^5 W cm^{-2}). Furthermore, as for two-photon excitation at 800 nm, the FCS data at any irradiance do not bear any triplet term, which suggests a negligible population of the triplet state. The curve, $N_F(I_{av})$, is well-described by Equations (9) and (10) using the known parameters taken from the cell bleaching and 515 nm experiments (compare Table 1, $\sigma_{01}(350\ nm) = 3.6\times10^{-17}$ cm^2, $k_0 = 2.56\times10^8$ s^{-1}, $k_f = 2.4\times10^8$ s^{-1}, $k_b = 795$ s^{-1}, $\sigma_{1n}(350\ nm) = 2.5\times10^{-16}$ cm^2, $k_{n1} = (200\ fs)^{-1}$, $k_{ISC} = 1.1\times10^6$ s^{-1}, and $k_{T1n} = 4.9\times10^5$ s^{-1}). A rate constant for photobleaching from the S_n state of $k_{bSn} = 3.75\times10^{10}$ s^{-1} is obtained, which is several orders of magnitude higher than that for excitation at 515 nm. For the quasi-continuous steady-state approach [Eq. (10)] a pulse enhancement factor of $g_p^{qcw} = 1.8$ [compare Eq. (7)] has to be introduced, in order to perfectly coincide with the exact calculations. Within the steady-state model this factor accommodates the fact that excitation is performed from a short-lived state (S_1, $S_{>1}$ or their higher vibronic states). Such excitation and subsequent bleaching is favored by the high photon flux densities of short, especially 180-fs pulses. Thus, the simplified steady-state model can well-describe the data, since no pulse saturation effects occur. The efficient excitation to S_n results in no noticeable population of the triplet state. Thus, in contrast to cw or picosecond-pulsed excitation to S_1 (502 to 528 nm), the main photolysis pathway in the case of using femtosecond pulses does not constitute the T_n state.

In conclusion, one-photon excitation with sub-picosecond pulses leads to a strong enhancement of the population of higher-excited singlet states. The higher photon energy, E_n (compare Table 1), at 350 nm results in secondary excitations of electronic states that are much closer to the ionization level and thus more photoreactive. The achievable maximum number of detected photons of $N_F < 3$ within an observation time of $t_{ob} = 0.41$ ms renders an accurate determination of temporal parameters such as k_z by an FCS experiment impossible. Single-molecule and FCS experiments should therefore circumvent the use of femtosecond pulsed-excitation in the UV region, which has already been stated previously.[63,75,98]

4. Conclusions

We have conducted photobleaching measurements of Rh6G in water under the conditions of one- and two-photon induced microscopy. The different excitation modes investigated include: 1) one-photon excitation into the S_1 state at 500 to 528 nm using continuous wave and picosecond-pulsed lasers; and 2) two- and one-photon excitation into higher-excited singlet states $S_{>1}(400)$ and $S_{>1}(350)$, respectively, using femtosecond excitation pulses. From single-molecule trajectories and FCS curves we extracted the photokinetic parameters based on a molecular rate equation analysis. The underlying theory presented, is based on simple assumptions of steady-state populations and quasi-continuous mean irradiances in the case of pulsed excitation. Comparisons to exact calculations show that the simplified model, nevertheless, describes all data remarkably well. The maximum achievable fluorescence photons from a single fluorophore have been determined for the different excitation modes. In all cases, the fluorescence is limited at high irradiances by photolysis from higher-excited electronic states, S_n and T_n, confirming previous observation.[42,43,51,54,55,57,63–65,67,68,70,72,80] The dependence of detectable fluorescence signal shows three regimes as exposed in Figure 2b: 1) linear dependence for low irradiances, 2) saturation to a maximum value due to triplet population and photobleaching, and 3) a decrease for high irradiances ($I_0 > 10^5$ W cm^{-2}), caused by the two-step photolysis from the higher-excited states, S_n and T_n. It was shown that this reactivity is more pronounced from the triplet state and increases with the photon energy of excitation, E_n (compare Table 1), as well as with the polarity of the solvent, thus, being sensitive to the environment. No difference in photobleaching was observed between cw and picosecond-pulsed excitation to the S_1 state, which is of great advantage for most time-resolved single-molecule applications. In contrast, in the case of femtosecond-pulsed excitation, the absorption at 500 to 528 nm to higher electronic states dominates all photophysical processes of the dye, such that the population of the triplet state is negligible. As a result, when compared to excitation to S_1, the maximum number of detected fluorescence photons, N_F (Table 1), is reduced by a factor of 180 and 18 for 350-nm one-photon excitation and 800-nm two-photon excitation with femtosecond pulses, respectively. Furthermore, the simple theoretical model applied can in principle explain any dependence of the bleaching reactivity on the irradiance by including an unlimited number of additional higher absorption steps.

For an optimized fluorescence yield, it is therefore advantageous to use picosecond laser pulses, as has been reported previously.[93,95] Furthermore, the applied irradiance and wave-

length should be chosen with care. The least irradiance for a sufficient fluorescence is needed for excitation at the maximum of the S_1 absorption band, which in turn renders the least photobleaching activity. Moving away towards more blue-shifted wavelength will suppress the fluorescence signal due to the higher irradiances required and the higher photon energies applied. Two-photon excitation, on the other hand, bears a trade-off between low off-focus and severe in-focus photobleaching. The high photon densities required for two-photon excitation will always deteriorate in-focus photochemistry. Moving towards stretched pulses or different pulse shapes could introduce some improvements not only in the context of fluorescence yield,[93–95,99] but also in view of cell damage.[100,101]

In summary, we have presented an experimental strategy in conjunction with a simple theoretical model, which allows quantifying molecular photobleaching parameters of fluorophores under typical conditions in confocal and two-photon induced fluorescence microscopy with continuous wave and pulsed excitation. We have unravelled the underlying mechanisms behind photobleaching for the different excitation modes, which enable us to optimize the observed fluorescence yield from a single fluorophore. Future studies will therefore involve these methods in the search of an optimized dye.

Experimental Section

The confocal epi-illuminated fluorescence microscope set up was described in detail elsewhere.[43,51,75] A passively mode-locked Ti:sapphire laser (Mira, Coherent) pumped by an Argon ion laser (Innova Sabre, Coherent) was applied for excitation at 350 nm (frequency-doubled 700 nm beam) or at 800 nm (pulse length of $\approx$200 fs and repetition rate of 76 MHz). The argon ion laser itself is used for excitation at 502, 515 and 528 nm either in the continuous wave (cw) or actively mode-locked pulsed mode (APE, Berlin, Germany; pulse length of $\approx$180 ps and repetition rate of 73 MHz). A water immersion objective (Olympus 60x, UPlanApo, N.A. 1.2) was used to focus the excitation beam into the sample solution and to collect the fluorescence light. Detection was done in a confocal arrangement using an avalanche photodiode (APD-AQR 15, EG&G Vandreuil, Quebec, Canada). All measurements were carried out on freely diffusing molecules in an open detection volume. The focal irradiance, I_0, was calculated from the average excitation power, P, and the focal $1/e^2$ radius, ω_0, as determined by fluorescence correlation spectroscopy of an aqueous Rhodamine 6G solution at low excitation power (see Eq. (10), $D = 3\times10^{-6}\,cm^2\,s^{-1}$); $I_0 = P/(\pi/2\,\omega_0^2)$.[43,88]

The dye Rhodamine 6G chloride (Rh6G; Radiant Dyes, Wermelskirchen, Germany) was diluted in double-distilled water (in ethanol (Merck, Darmstadt, Germany) or glycerine (Fluka, Buchs, CH)) to a final concentration of $\approx10^{-7}$, $\approx10^{-9}$ and $\approx10^{-12}$ M for the ensemble bleaching studies at low irradiances, FCS measurements and single-molecule experiments, respectively. The absorption spectrum was measured in a 1×1 cm quartz suprasil cell (Hellma, Mühlheim, Germany) with a Cary-5E UV/Vis–near-IR spectrometer (Varian, Mulgrave, Australia) at a known dye concentration. All measurements were taken at ambient temperature in a lab conditioned at 20 °C.

Acknowledgements

We thank Volodymyr Kudryavtsev and Opas Tojira for measuring the anisotropy spectrum of Rh6G and Jörg Schaffer for helping with the two-photon set up.

Keywords: fluorescence correlation spectroscopy · fluorescence spectroscopy · multiphoton excitation · photochemistry · single-molecule studies

[1] W. Denk, J. H. Strickler, W. W. Webb, *Science* **1990**, *248*, 73.
[2] R. Kühnemuth, C. A. M. Seidel, *Single Mol.* **2001**, *2*, 251.
[3] R. Y. Tsien, *Annu. Rev. Biochem.* **1998**, *67*, 509.
[4] S. W. Hell, *Nat. Biotechnol.* **2003**, *21*, 1347.
[5] R. Neher, E. Neher, *J. Microsc.* **2004**, *213*, 46.
[6] *Handbook of Biological Confocal Microscopy* (Ed.: J. Pawley), Plenum Press, New York, **1995**.
[7] K. König, *J. Microsc.* **2000**, *200*, 83.
[8] F. Helmchen, W. Denk, *Curr. Opin. Neurobiol.* **2002**, *12*, 593.
[9] X. Michalet, A. N. Kapanidis, T. Laurence, F. Pinaud, S. Doose, M. Pflughoefft, S. Weiss, *Ann. Rev. Biophys. Biomol. Struct.* **2003**, *32*, 161.
[10] E. B. Shera, N. K. Seitzinger, L. M. Davis, R. A. Keller, S. A. Soper, *Chem. Phys. Lett.* **1990**, *174*, 553.
[11] R. Rigler, Ü. Mets, J. Widengren, P. Kask, *Eur. Biophys. J.* **1993**, *22*, 169.
[12] M. Eigen, R. Rigler, *Proc. Natl. Acad. Sci. USA* **1994**, *91*, 5740.
[13] S. Nie, D. T. Chiu, R. N. Zare, *Anal. Chem.* **1995**, *67*, 2849.
[14] C. Zander, M. Sauer, K. H. Drexhage, D. S. Ko, A. Schulz, J. Wolfrum, L. Brand, C. Eggeling, C. A. M. Seidel, *Appl. Phys. B* **1996**, *63*, 517.
[15] A. A. Deniz, M. Dahan, J. R. Grunwell, T. Ha, A. E. Faulhaber, D. S. Chemla, S. Weiss, P. G. Schultz, *Proc. Natl. Acad. Sci. USA* **1999**, *96*, 3670.
[16] W. P. Ambrose, P. M. Goodwin, J. H. Jett, A. van Orden, H. J. Werner, R. A. Keller, *Chem. Rev.* **1999**, *99*, 2929.
[17] D. Magde, E. L. Elson, W. W. Webb, *Phys. Rev. Lett.* **1972**, *29*, 705.
[18] R. Rigler, E. L. Elson in *Chemical Physics* (Eds.: F. P. Schäfer, J. P. Toennies, W. Zinth), Springer, Berlin, Heidelberg, **2001**.
[19] J. R. Fries, L. Brand, C. Eggeling, M. Köllner, C. A. M. Seidel, *J. Phys. Chem. A* **1998**, *102*, 6601.
[20] P. Kask, K. Palo, D. Ullmann, K. Gall, *Proc. Natl. Acad. Sci. USA* **1999**, *96*, 13756.
[21] Y. Chen, J. D. Müller, P. T. C. So, E. Gratton, *Biophys. J.* **1999**, *77*, 553.
[22] J. R. Lakowicz, H. Szmaczinski, K. Nowaczyk, *Proc. Natl. Acad. Sci. USA* **1992**, *89*, 1271.
[23] A. Draaijer, R. Sanders, H. C. Gerritsen in *Handbook of Biological Confocal Microscopy* (Ed.: J. Pawley), Plenum Press, New Yourk, **1995**.
[24] R. M. Clegg, P. C. Schneider in *Fluorescence Microscopy and Fluorescent Probes* (Ed.: J. Slavik), Plenum Press, **1996**, pp. 15.
[25] A. Schönle, M. Glatz, S. W. Hell, *Appl. Opt.* **2000**, *39*, 6306.
[26] S. Jakobs, V. Subramaniam, A. Schönle, T. M. Jovin, S. W. Hell, *FEBS Lett.* **2000**, *479*, 131.
[27] D. Axelrod, P. Ravdin, D. E. Koppel, J. Schlessinger, W. W. Webb, E. L. Elson, T. R. Podleski, *Proc. Natl. Acad. Sci. USA* **1976**, *73*, 4594.
[28] Edidin, M. , Y. Zagyansky, T. J. Lardner, *Science* **1976**, *191*, 466.
[29] J. R. Lakowicz in *Topics in Fluorescence Spectroscopy, Vol.* 1, Plenum Press, New York, **1991**.
[30] C. Eggeling, S. Berger, L. Brand, J. R. Fries, J. Schaffer, A. Volkmer, C. A. M. Seidel, *J. Biotechnol.* **2001**, *86*, 163.
[31] A. Gaiduk, R. Kühnemuth, M. Antonik, C. A. M. Seidel, *ChemPhysChem* **2005**, *6*, 976.
[32] P. J. Rothwell, S. Berger, O. Kensch, S. Felekyan, M. Antonik, B. M. Wöhrl, T. Restle, R. S. Goody, C. A. M. Seidel, *Proc. Natl. Acad. Sci. USA* **2003**, *100*, 1655.
[33] M. Margittai, E. Schweinberger, J. Widengren, D. Fasshauer, G. Schröder, E. Haustein, S. Felekyan, M. König, H. Grubmüller, R. Jahn, C. A. M. Seidel, *Proc. Natl. Acad. Sci. USA* **2003**, *100*, 15516.
[34] M. Diez, B. Zimmermann, M. Börsch, M. König, E. Schweinberger, S. Steigmiller, R. Reuter, S. Felekyan, V. Kudryavtsev, C. A. M. Seidel, P. Gräber, *Nat. Struct. Mol. Biol.* **2004**, *11*, 135.

[35] M. Göppert-Mayer, *Ann.Phys.* **1931**, *9*, 273.
[36] C. Xu, W. W. Webb, *J. Opt. Soc. Am. B* **1996**, *13*, 481.
[37] S. W. Hell, K. Bahlmann, M. Schrader, A. Soini, H. Malak, I. Gryczinski, J. R. Lakowicz, *J. Biomed. Opt.* **1996**, *1*, 71.
[38] W. R. Zipfel, R. M. Williams, R. Christie, A. Y. Nikitin, B. T. Hyman, W. W. Webb, *Proc. Natl. Acad. Sci. USA* **2003**, *100*, 7075.
[39] K. G. Heinze, A. Koltermann, P. Schwille, *Proc. Natl. Acad. Sci. USA* **2000**, *97*, 10377.
[40] S. A. Kim, P. Schwille, *Curr. Opin. Neurobiol.* **2003**, *13*, 583.
[41] R. Y. Tsien, A. Waggoner in *Handbook of Biological Confocal Microscopy* (Ed.: J. Pawley), Plenum Press, New York, **1995**, pp. 267.
[42] C. Eggeling, J. Widengren, R. Rigler, C. A. M. Seidel in *Applied fluorescence in chemistry, biology and medicine* (Eds.: W. Rettig, B. Strehmel, M. Schrader, H. Seifert), Springer, Berlin, **1999**, pp. 193.
[43] C. Eggeling, J. Widengren, R. Rigler, C. A. M. Seidel, *Anal. Chem.* **1998**, *70*, 2651.
[44] D. Beer, J. Weber, *Opt. Commun.* **1972**, *5*, 307.
[45] V. E. Korobov, A. K. Chibisov, *J. Photochem.* **1978**, *9*, 411.
[46] I. Rosenthal, *Opt. Commun.* **1978**, *24*, 164.
[47] S. A. Soper, H. L. Nutter, R. A. Keller, L. M. Davis, E. B. Shera, *Photochem. Photobiol.* **1993**, *57*, 972.
[48] A. Mills, A. Belghazi, R. H. Davies, D. Worsley, S. Morris, *J. Photochem. Photobiol. A* **1994**, *79*, 131.
[49] E. Thiel, Habilitation thesis, Universität-GH Siegen (Siegen, Germany), **1995**.
[50] J. Widengren, Ü. Mets, R. Rigler, *J. Phys. Chem.* **1995**, *99*, 13368.
[51] J. Widengren, R. Rigler, *Bioimaging* **1996**, *4*, 149.
[52] J. P. Crimaldi, *Exp. Fluids* **1997**, *23*, 325.
[53] S. C. Hill, M. D. Barnes, N. Lermer, W. B. Whitten, J. M. Ramsey, *Anal. Chem.* **1998**, *70*, 2964.
[54] J. Mertz, *Eur. Phys. J. D* **1998**, *3*, 53.
[55] L. A. Deschenes, D. A. Vanden Bout, *Chem. Phys. Lett.* **2002**, *365*, 387.
[56] R. Zondervan, F. Kulzer, S. B. Orlinskii, M. Orrit, *J. Phys. Chem. A* **2003**, *107*, 6770.
[57] R. Zondervan, F. Kulzer, M. A. Kolchenko, M. Orrit, *J. Phys. Chem. A* **2004**, *108*, 1657.
[58] M. Anbar, E. Hart, *J. Am. Chem. Soc.* **1964**, *86*, 5633.
[59] E. Hart, M. Anbar, *The Hydrated Electron*, Wiley Interscience, New York, **1970**.
[60] D. N. Nikogosyan, *Laser Chem.* **1987**, *7*, 29.
[61] E. V. Khoroshilova, D. N. Nikogosyan, *J. Photochem. Photobiol. B* **1990**, *5*, 413.
[62] A. Reuther, D. N. Nikogosyan, A. Laubereau, *J. Phys. Chem.* **1996**, *100*, 5570.
[63] C. Eggeling, L. Brand, C. A. M. Seidel, *Bioimaging* **1997**, *5*, 105.
[64] G. H. Patterson, D. W. Piston, *Biophys. J.* **2000**, *78*, 2159.
[65] R. Niesner, W. Roth, K. H. Gericke, *ChemPhysChem* **2004**, *5*, 678.
[66] A. V. Aristov, *Opt. Spectrosc.* **1994**, *77*, 856.
[67] P. S. Dittrich, P. Schwille, *Appl. Phys. B* **2001**, *73*, 829.
[68] T.-S. Chen, S.-Q. Zeng, Q.-M. Luo, Z.-H. Zhang, W. Zhou, *Biophys. Biochem. Res. Commun.* **2002**, *291*, 1272.
[69] W. P. Ambrose, P. M. Goodwin, J. C. Martin, R. A. Keller, *Phys. Rev. Lett.* **1994**, *72*, 160.
[70] E. J. Sanchez, L. Novotny, G. R. Holtom, X. S. Xie, *J. Phys. Chem A* **1997**, *101*, 7019.
[71] M. Sonnleitner, G. J. Schütz, T. Schmidt, *Chem. Phys. Lett.* **1999**, *300*, 221.
[72] M. Lippitz, W. Erker, H. Decker, K. E. van Holde, T. Basche, *Proc. Natl. Acad. Sci. USA* **2002**, *99*, 2772.
[73] G. Chirico, F. Cannone, A. Diaspro, *J. Phys. D* **2003**, *36*, 1682.
[74] A. Fischer, C. Cremer, E. H. K. Stelzer, *Appl. Opt.* **1995**, *34*, 1989.
[75] L. Brand, C. Eggeling, C. Zander, K. H. Drexhage, C. A. M. Seidel, *J. Phys. Chem. A* **1997**, *101*, 4313.
[76] S. Reindl, A. Penzkofer, *Chem. Phys.* **1996**, *211*, 431.
[77] R. A. Mathies, K. Peck, L. Stryer, *Anal. Chem.* **1990**, *62*, 1786.
[78] L. Song, E. J. Hennink, I. T. Young, H. J. Tanke, *Biophys. J.* **1995**, *68*, 2588.
[79] J. Enderlein, D. L. Robbins, W. P. Ambrose, P. M. Goodwin, R. A. Keller, *Bioimaging* **1997**, *5*, 88.
[80] A. Molski, *J. Chem. Phys.* **2001**, *114*, 1142.
[81] T. Hirschfeld, *Appl. Opt.* **1976**, *15*, 3135.
[82] C. Eggeling, PhD thesis, Georg-August-Universität Göttingen (Göttingen, Germany), **1999**.
[83] D. E. Koppel, *Phys. Rev. A* **1974**, *10*, 1938.
[84] K. H. Drexhage, in *Dye Lasers* (Ed.: F. P. Schäfer), Springer-Verlag, Berlin, **1973**, pp. 144.
[85] C. Zander, K. H. Drexhage in *Advances in Photochemistry, Vol.* 20 (Eds.: D. C. Neckers, D. H. Volman, G. von Bünau), John Wiley & Sons Inc, New York, **1995**, pp. 59.
[86] M. C. Gazeau, V. Wintgens, P. Valat, J. Kossanyi, D. Doizi, G. Salvetat, J. Jaraudias, *Can. J. Phys.* **1993**, *71*, 59.
[87] I. Gregor, M. Heupel, E. Thiel, *Chem. Phys.* **2001**, *272*, 185.
[88] R. L. Hansen, X. R. Zhu, J. M. Harris, *Anal. Chem.* **1998**, *70*, 1281.
[89] G. Nishimura, M. Kinjo, *Anal. Chem.* **2004**, *76*, 1963.
[90] K. Berland, G. Shen, *Appl. Opt.* **2003**, *42*, 5566.
[91] J. Enderlein, I. Gregor, D. Patra, J. Fitter, *Curr. Pharm. Biotechnol.* **2004**, *5*, 155.
[92] I. Gregor, D. Patra, J. Enderlein, *ChemPhysChem* **2004**, *5*, 1.
[93] J. Bewersdorf, S. W. Hell, *J. Microsc.* **1998**, *191*, 28.
[94] M. J. Booth, S. W. Hell, *J. Microsc.* **1998**, *190*, 298.
[95] M. Dyba, S. W. Hell, *Appl. Opt.* **2003**, *42*, 5123.
[96] A. Schönle, S. W. Hell, *Opt. Lett.* **1998**, *23*, 325.
[97] J. Mertz, C. Xu, W. W. Webb, *Opt. Lett.* **1995**, *20*, 2532.
[98] S. Wennmalm, H. Blom, L. Wallerman, R. Rigler, *Biol. Chem.* **2001**, *382*, 393.
[99] H. Kawano, Y. Nabekawa, A. Suda, Y. Oishi, H. Mizuno, A. Miyawaki, K. Midorikawa, *Biochem. Biophys. Res. Commun.* **2003**, *311*, 592.
[100] K. König, T. W. Becker, P. Fischer, I. Riemann, K.-J. Halbhuber, *Opt. Lett.* **1999**, *24*, 113.
[101] A. Hopt, E. Neher, *Biophys. J.* **2001**, *80*, 2029.

Received: October 24, 2004
Revised: March 4, 2005

